Materials Research Bulletin 135 (2021) 111116

Contents lists available at ScienceDirect

Materials Research Bulletin

journal homepage: www.elsevier.com/locate/matresbu

Structure, electrical conductivity, and Raman spectra of $(Cu_{1-x}Ag_x)_7GeS_5I$ and $(Cu_{1-x}Ag_x)_7GeSe_5I$ mixed crystals

I.P. Studenyak [a,*], A.I. Pogodin [a], V.I. Studenyak [a], M.J. Filep [a], O.P. Kokhan [a], P. Kúš [b], Y. M. Azhniuk [a,c], D.R.T. Zahn [d]

[a] Uzhhorod National University, 46 Pidhirna Str., 88000 Uzhhorod, Ukraine
[b] Comenius University, Mlynska Dolina, 84248 Bratislava, Slovakia
[c] Institute of Electron Physics, Ukr. Nat. Acad. Sci., Universytetska Str. 21, Uzhhorod 88017, Ukraine
[d] Semiconductor Physics, Chemnitz University of Technology, D-09107 Chemnitz, Germany

ARTICLE INFO

Keywords:
Mixed crystals
Electrical conductivity
Fast-ion conductors
Raman spectroscopy

ABSTRACT

The structure of $(Cu_{1-x}Ag_x)_7GeSe_5I$ mixed crystals with $Cu^+ \leftrightarrow Ag^+$ substitution is described and compared to $(Cu_{1-x}Ag_x)_7GeS_5I$ employing the results of X-ray diffraction (XRD) and the atomic coordinates by Rietveld refinement. Based on the electrical measurements, the compositional behaviour of ionic and electronic conductivity as well as the ratio of ionic and electronic components of conductivity for $(Cu_{1-x}Ag_x)_7GeS_5I$ and $(Cu_{1-x}Ag_x)_7GeSe_5I$ is discussed. Raman spectra of $(Cu_{1-x}Ag_x)_7GeSe_5I$ and $(Cu_{1-x}Ag_x)_7GeSe_5I$ are consistent with the XRD data regarding their cubic structure. A one-mode compositional behaviour of the most prominent peak (corresponding to the vibrations of GeS_4 or $GeSe_4$ tetrahedra) under Cu→Ag cation substitution is observed, an unexpectedly strong shift of the peak frequency with x reveals its marked effect on the dynamics of GeS_4 or $GeSe_4$ tetrahedra. Compounds with high Ag content undergo photochemical surface transformations under laser irradiation during Raman measurements.

1. Introduction

The large family of argyrodite crystals is characterised by a common chemical formula $A^{m+1}_{(12-n-x)/m}B^{n+}X^{2-}_{6-x}Y^{1-}$ ($0< x <1$) with mono- or divalent cations A and cations B with higher valence as well as chalcogens X and halogens Y. It includes numerous materials with structures ranging from cubic to monoclinic [1,2]. Lithium- [3–8], copper- [9–12], and silver-containing [13–16] argyrodites are known for high ionic conductivity and are promising for solid-electrolyte accumulators, supercapacitors, and electrochemical sensors. Composites, ceramics as well as thin films based on these materials were prepared for application purposes [10,12,17,18]. Cu_7GeS_5I and Ag_7GeS_5I compounds as well as their selenium-containing counterparts Cu_7GeSe_5I and Ag_7GeSe_5I belong to the argyrodite family and possess high ionic conductivity [9,11,15,16,19,20]. The total electric conductivity of $(Cu_{1-x}Ag_x)_7GeS_5I$ mixed crystals was found to exhibit a non-monotonous compositional behaviour with a minimum at $x = 0.75$ [15]. For $(Cu_{1-x}Ag_x)_7GeSe_5I$ the compositional dependence of the ionic conductivity is non-monotonous with a maximum near $x = 0.5$, whereas the electronic conductivity for $(Cu_{1-x}Ag_x)_7GeSe_5I$ mixed crystals nonlinearly decreases with x [16].

Important information with regard to the crystalline structure can be acquired from Raman spectroscopy. Among the crystals from the argyrodite family, vibrational spectra of phosphorus-based compounds with copper cation Cu_6PS_5Hal (Hal = Cl, Br, I) were studied most extensively [21–24]. Meanwhile, to our knowledge, the Raman spectra of $(Cu_{1-x}Ag_x)_7GeS_5I$ and $(Cu_{1-x}Ag_x)_7GeSe_5I$ mixed crystals have not been reported so far. Here we present a study of X-ray diffraction, Raman spectra, and electrical characteristics of germanopentasulphoiodide $(Cu_{1-x}Ag_x)_7GeS_5I$ and germanopentaselenoiodide $(Cu_{1-x}Ag_x)_7GeSe_5I$ argyrodites with Cu→Ag substitution.

2. Materials and methods

Cu_7GeS_5I, Cu_7GeSe_5I, Ag_7GeS_5I, and Ag_7GeSe_5I crystals were obtained by directed crystallization from the melt while $(Cu_{1-x}Ag_x)_7GeS_5I$ and $(Cu_{1-x}Ag_x)_7GeSe_5I$ mixed crystals on their base were obtained by vertical zone crystallization from the melt (for details see our recent studies [15,16]).

* Corresponding author.
E-mail address: studenyak@dr.com (I.P. Studenyak).

https://doi.org/10.1016/j.materresbull.2020.111116
Received 3 August 2020; Received in revised form 22 September 2020; Accepted 12 October 2020
Available online 14 November 2020

The analysis of the mechanism of $Cu^{+}\leftrightarrow Ag^{+}$ substitution and the calculation of atomic coordinates in the unit cell was carried out using the Rietveld refinement method [25,26]. The experimental data were obtained using a DRON 4-07 diffractometer (Cu Kα radiation, 2Θ angle scanning step 0.02°, acquisition time 1 s). The calculation and refinement of the structural models were performed using EXPO 2014 software [27,28], while the VESTA 3.4.4 software [29] was used for visualisation.

The electrical conductivity of $(Cu_{1-x}Ag_x)_7GeS_5I$ mixed crystals was investigated by impedance spectroscopy in the frequency range of 10 Hz – 3×10^5 Hz using a high-precision AT 2818 LCR meter. The AC amplitude was 10 mV. $(Cu_{1-x}Ag_x)_7GeS_5I$ single crystal samples for the measurements were prepared in the shape of rectangular parallelepipeds with lateral area $S = 0.560–0.315$ cm^2 and thickness $l = 0.150–0.221$ cm. The measurements were carried out by a two-electrode method with blocking gold contacts. The gold contacts were deposited by chemical precipitation from solutions.

Raman spectra of $(Cu_{1-x}Ag_x)_7GeS_5I$ and $(Cu_{1-x}Ag_x)_7GeSe_5I$ mixed crystals were measured at room temperature using a Horiba LabRAM 800 spectrometer. Excitation was provided by solid-state lasers (488.0 and 514.7 nm) or a He–Ne laser (632.8 nm). The scattered light was detected by a cooled CCD camera. The instrumental resolution was better than 2.5 cm^{-1}.

3. Results and discussion

3.1. Crystal structure

Cu_7GeS_5I, Cu_7GeSe_5I, Ag_7GeS_5I, and Ag_7GeSe_5I compounds are known to crystallise with a face-centred cubic cell of the argyrodite structure (F–43m space group, Z = 4) with lattice parameters $a = 9.9669(5)$ Å for Cu_7GeS_5I, $a = 10.3598(5)$ Å for Cu_7GeSe_5I, $a = 10.6691(1)$ for Ag_7GeS_5I, and $a = 10.9884(2)$ for Ag_7GeSe_5I [2,13,14,23,30–32]. Continuous rows of solid solutions are formed in the Cu_7GeS_5I–Ag_7GeS_5I and Cu_7GeSe_5I–Ag_7GeSe_5I systems by $Cu^{+}\leftrightarrow Ag^{+}$ substitution.

Fig. 1 shows an example of a Rietveld plot for the $(Cu_{0.5}Ag_{0.5})_7GeSe_5I$ solid solution crystal. The X-ray diffractogram calculated from the refinement results (the red curve) is in a good agreement with the experimentally observed one (blue curve). The violet curve shows the difference between the refinement and the experiment.

The Rietveld refinement analysis enabled us to confirm the lattice parameter values for the end-point Cu_7GeS_5I, Cu_7GeSe_5I, Ag_7GeS_5I, and Ag_7GeSe_5I compounds as well as to determine the lattice parameter values for $Cu_{1-x}Ag_x)_7GeS_5I$ ($x = 0.25, 0.5, 0.75$) and $(Cu_{1-x}Ag_x)_7GeSe_5I$ ($x = 0.25, 0.5, 0.75$) mixed crystals (Fig. 2). For the Cu_7GeS_5I–Ag_7GeS_5I system the lattice parameter varies with composition with a slight downward bowing while for $(Cu_{1-x}Ag_x)_7GeSe_5I$ mixed crystals a linear dependence is observed in accordance with the Vegard law.

The study of the structure of $(Cu_{1-x}Ag_x)_7GeS_5I$ mixed crystals and the analysis of structural units of its anionic core were performed in our earlier paper [33]. Therefore, here we pay more detailed attention to the Cu_7GeSe_5I–Ag_7GeSe_5I system. The unit cell contains two symmetrically distinct selenium positions Se1 (4c) and Se2 (16e), one position of germanium Ge1 (4b) and one iodine I1 (4a), for which the site occupancy factor (SOF) is 1. Base units of the anionic core of $(Cu_{1-x}Ag_x)_7GeSe_5I$ crystals are $[GeSe_4]$, $[Se_3I]$, and $[SeI_4]$ tetrahedra, on the faces and in the centre of which copper and/or silver atoms are located (Fig. 3). In the structure of Cu_7GeSe_5I and Ag_7GeSe_5I the $[GeSe_4]$ tetrahedron is symmetric, *i.e.* the Ge atom is in an absolutely central position, Ge–Se bond lengths for Cu_7GeSe_5I are 2.144 Å, Se–Se distances are 3.502 Å, the tetrahedron volume is 5.06 $Å^3$ while for Ag_7GeSe_5I these values are 2.240 Å, 3.658 Å, and 5.77 $Å^3$, respectively. Similar to Cu_7GeSe_5I and Ag_7GeSe_5I, in mixed $(Cu_{1-x}Ag_x)_7GeSe_5I$ crystals the $[GeSe_4]$ tetrahedra remain symmetric (Fig. 3). The Ge–Se bond lengths, Se–Se distances, and the tetrahedra volumes for the $(Cu_{1-x}Ag_x)_7GeSe_5I$ mixed crystals are listed in Table 1.

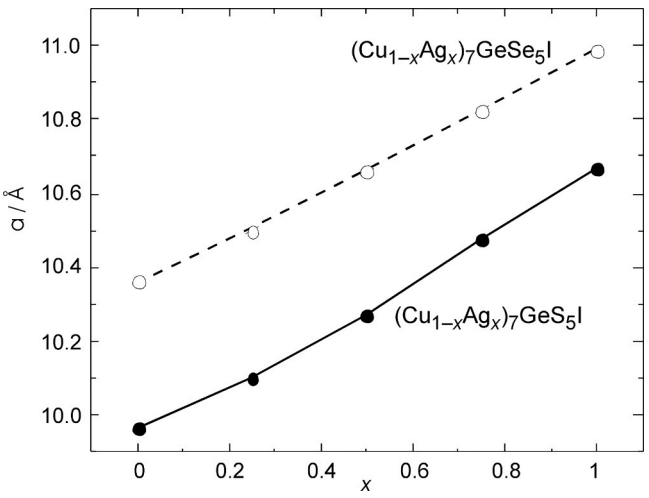

Fig. 2. Compositional dependence of the lattice parameter for the $(Cu_{1-x}Ag_x)_7GeS_5I$ and $(Cu_{1-x}Ag_x)_7GeSe_5I$ mixed crystals. The errors of the lattice parameter determination are below the symbol size.

A comparison of $(Cu_{1-x}Ag_x)_7GeS_5I$ and $(Cu_{1-x}Ag_x)_7GeSe_5I$ mixed crystals shows that the main parameters related to the anionic core at $Cu^{+}\leftrightarrow Ag^{+}$ substitution behave similarly as revealed by a similar monotonous compositional behaviour of the lattice parameters (Fig. 2), densities, etc. A more complicated behaviour is observed when the mobile cationic sublattice is considered. For $(Cu_{1-x}Ag_x)_7GeS_5I$ mixed crystals the $Cu^{+}(Ag^{+})$ ion mobility in the cationic sublattice is smaller than for the end-point compounds, which follows from the higher site occupancy factor (SOF) in the mixed crystals (Fig. 4a). On the contrary, for $(Cu_{1-x}Ag_x)_7GeSe_5I$ mixed crystals the mobility of the cationic sublattice increases (the SOF decreases) with respect to that of the end-point

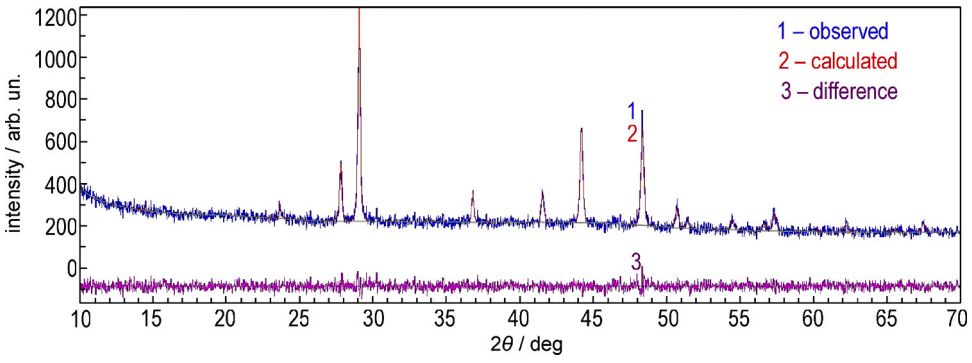

Fig. 1. Rietveld refinement plot for the X-ray diffractogram of $(Cu_{0.5}Ag_{0.5})_7GeSe_5I$ solid solution crystal.

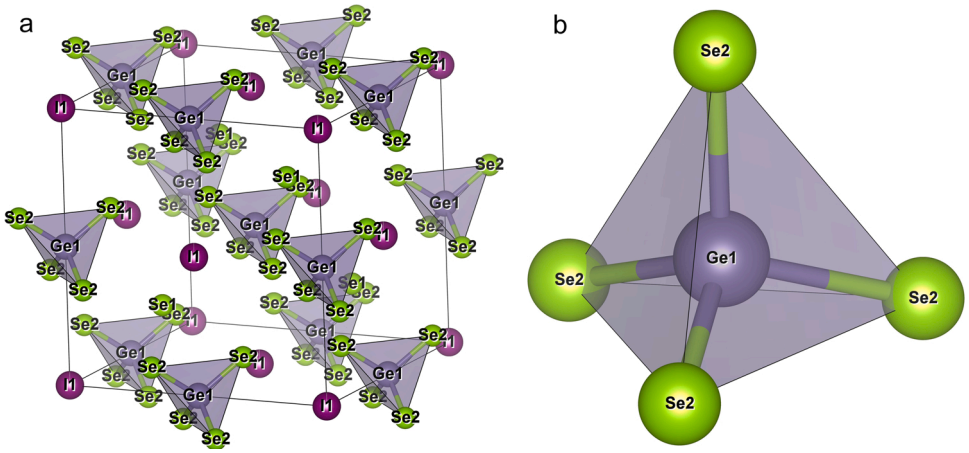

Fig. 3. Unit cell (a) and [$GeSe_4$] tetrahedron (b) in the structure of $(Cu_{0,5}Ag_{0,5})_7GeSe_5I$ mixed crystals.

Table 1
Ge–Se bond lengths, Se–Se distances, and tetrahedra volumes for $(Cu_{1-x}Ag_x)_7GeSe_5I$ mixed crystals.

Compound	Ge–Se, Å	Se–Se, Å	V_{tet}, Å^3
Cu_7GeSe_5I	2.144	3.502	5.06
$(Cu_{0,75}Ag_{0,25})_7GeSe_5I$	2.149	3.510	5.10
$(Cu_{0,5}Ag_{0,5})_7GeSe_5I$	2.227	3.637	5.67
$(Cu_{0,25}Ag_{0,75})_7GeSe_5I$	2.269	3.705	5.99
Ag_7GeSe_5I	2.240	3.658	5.77

crystals (Fig. 4b). A similar behaviour is observed for the distances between the $Cu^+(Ag^+)$ mobile positions: for the sulphur-containing system an increase of maximal distances between the $Cu^+(Ag^+)$ mobile ion positions is observed for the mixed crystals (Fig. 4a) while for the selenium-containing system an opposite dynamics is observed (Fig. 4b).

One may thus conclude that the cationic sublattice of the mixed $(Cu_{1-x}Ag_x)_7Ge[S(Se)]_5I$ crystals is formed in a rather complicated way. In the mixed crystals, ion transport can be either enhanced (due to an increasing mobility and decreasing distances), or weakened (decreasing mobility and increasing distances), which actually occurs in both systems, but in different compositional intervals. It is especially noticeable for $(Cu_{0.25}Ag_{0.75})_7GeS_5I$ and $(Cu_{0.5}Ag_{0.5})_7GeSe_5I$ mixed crystals, for which a minimum and a maximum, respectively, are observed in the compositional dependences of the ionic conductivity.

3.2. Electrical conductivity

Our earlier papers were devoted to the study of the electrical conductivity of mixed $(Cu_{1-x}Ag_x)_7GeS_5I$ [15] and $(Cu_{1-x}Ag_x)_7GeSe_5I$ [16]. As mentioned above, for $(Cu_{1-x}Ag_x)_7GeS_5I$ only total electrical conductivity was investigated [15] while for $(Cu_{1-x}Ag_x)_7GeSe_5I$ the ionic and electronic components of the total electrical conductivity were separated [16]. Here, in order to check how the electrical properties change from the sulphur-containing $(Cu_{1-x}Ag_x)_7GeS_5I$ to the selenium-containing $(Cu_{1-x}Ag_x)_7GeSe_5I$ crystals, we present additional data which enabled us to separate the ionic and electronic components of the total conductivity. Note that for all single crystals of the $(Cu_{1-x}Ag_x)_7GeS_5I$ and $(Cu_{1-x}Ag_x)_7GeSe_5I$ systems the total electrical conductivity increases with frequency, typically for ion-conductive solids [15, 16]. For detailed studies of the frequency behaviour of the electric conductivity and for its separation into ionic and electronic components, a standard approach using electrode equivalent circuits (EECs) [34] and their analysis using Nyquist plots was applied. The parasitic inductance of the cell ($\sim 2 \times 10^{-8}$ H) is taken into account during the analysis of all samples. Note that detailed studies of the electric conductivity of $(Cu_{1-x}Ag_x)_7GeSe_5I$ solid solutions and there analysis using Nyquist plots

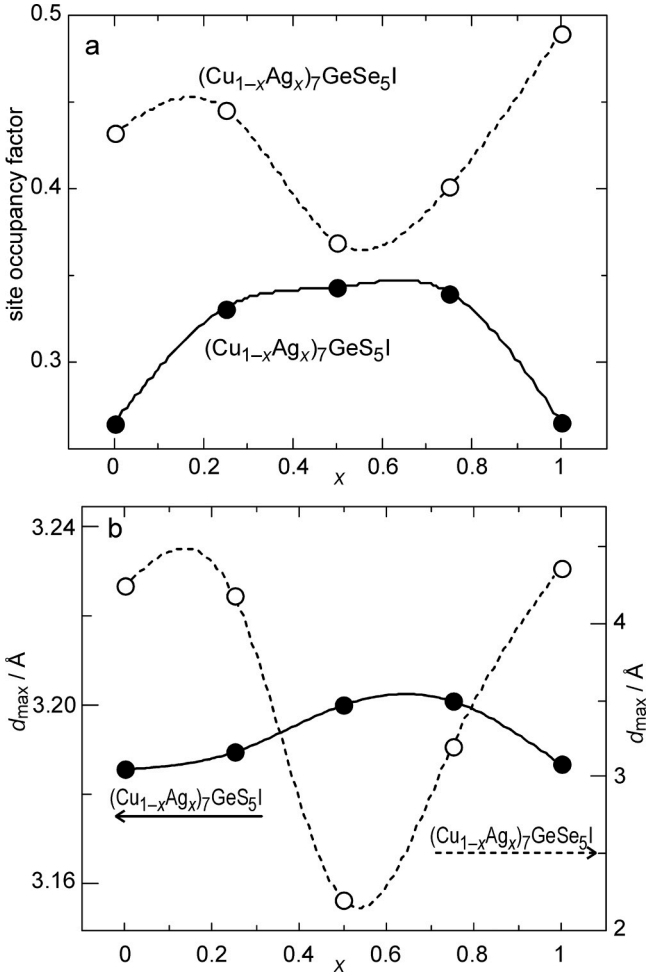

Fig. 4. Dependences of the SOF for mobile atoms (a) and the maximal distance between the $Cu^+(Ag^+)$ mobile ion positions in the cationic sublattice (b) on the $(Cu_{1-x}Ag_x)_7GeS_5I$ and $(Cu_{1-x}Ag_x)_7GeSe_5I$ mixed crystal composition.

in order to determine the contributions of the ionic and electronic components in the electric conductivity was performed in our earlier study [16].

For both the end-point Cu_7GeS_5I and Ag_7GeS_5I crystals and the $(Cu_{1-x}Ag_x)_7GeS_5I$ solid solutions ($x = 0.25$, 0.5, 0.75) two semicircles are observed in Nyquist plots in the frequency range under study.

Separation of contributions to the electric conductivity can be explained by an example of Nyquist plot analysis for $(Cu_{0.5}Ag_{0.5})_7GeS_5I$ mixed crystal.

Lower-frequency semicircles in the Nyquist plots are determined by diffusion relaxation processes at the electrode/crystal boundary and the electronic component of the conductivity what corresponds to a double diffusion layer capacitance C_d included in the EEC in parallel to the resistance R_e (Fig. 5). Besides, in course of the $Cu^+ \rightarrow Ag^+$ cationic substitution the lower-frequency semicircle is shifted towards lower frequencies which can be related to an increasing effect of ion diffusion processes due to a decreasing electronic component of the conductivity and, as a consequence, an increasing ion relaxation time.

Higher-frequency semicircles are characterised by ionic conductivity at domain boundaries which in the EEC corresponds to an ionic resistance R_{db} with a domain boundary capacitance C_{db} connected in parallel. An electronic resistance R_e is connected in parallel to them in the EEC (Fig. 5). Hence, the ionic component of the conductivity is determined by the domain boundary resistance R_{db} and the electronic one by R_e.

Analysis of the impedance spectra by means of EEC was performed for all the $(Cu_{1-x}Ag_x)_7GeS_5I$ crystals. It is observed that with increasing temperature the increase of the electronic conductivity gradually counterbalances the effect of ion diffusion processes at the domain boundaries which is evidenced by a decrease of the higher-frequency semicircle at 323 K. With further increase of temperature to 373 K the effect of ion diffusion processes further decreases and this, together with a decrease of the double diffusion layer finally results in a complete vanishing of the higher-frequency semicircle. One should note that the presence of domains can be related to the presence of a mosaic texture in the crystals under study, the domain boundaries being structural inhomogeneities revealed in misorientation of the texture elements [35].

Compositional dependences of both the ionic and the electronic conductivity are presented in Fig. 6. With $Cu^+ \rightarrow Ag^+$ cationic substitution the ionic component of the electric conductivity for the two mixed crystal systems behaves non-monotonously, but in a different way, exhibiting a minimum near $x = 0.75$ for $(Cu_{1-x}Ag_x)_7GeS_5I$ and a maximum near $x = 0.5$ for $(Cu_{1-x}Ag_x)_7GeSe_5I$ (Fig.6**a**).

An attempt to explain the mechanism of the electric conductivity and the specific features of the compositional behaviour of the ionic and electronic conductivity components for the $(Cu_{1-x}Ag_x)_7GeSe_5I$ solid solutions can be made based on the peculiarities of their crystal structure. In order to explain structural changes at $Cu^+ \leftrightarrow Ag^+$ substitution consider doubled $[Cu(Ag)Se_3I_2]$ tetrahedra. In the Cu_7GeSe_5I structure there are two symmetrically independent copper atoms in Cu1(24 g) and Cu2 (48 h) positions, the Cu1 position being trigonally coordinated by selenium atoms Se2Se2Se1 while the Cu2 atom is tetrahedrally coordinated

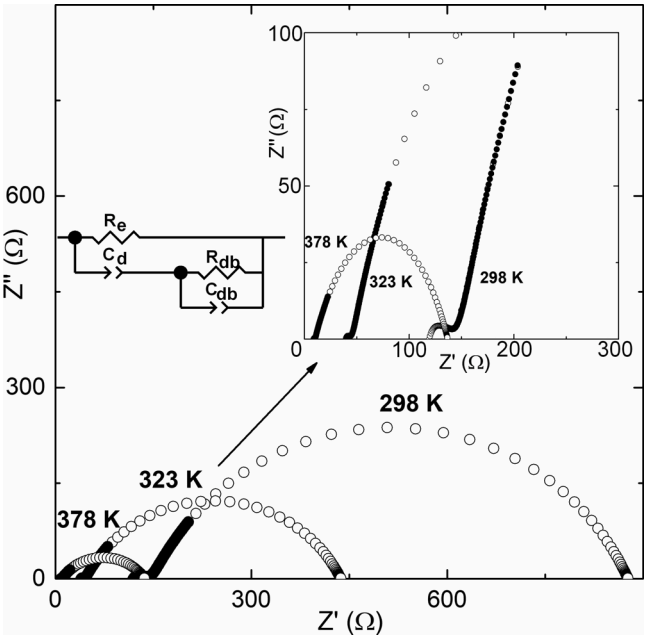

Fig. 5. Nyquist plots in Z'-Z'' coordinates for different temperatures: experimental data (black ciecles), calculation data (open circles), and the EEC for the $(Cu_{0.5}Ag_{0.5})_7GeS_5I$ mixed crystal.

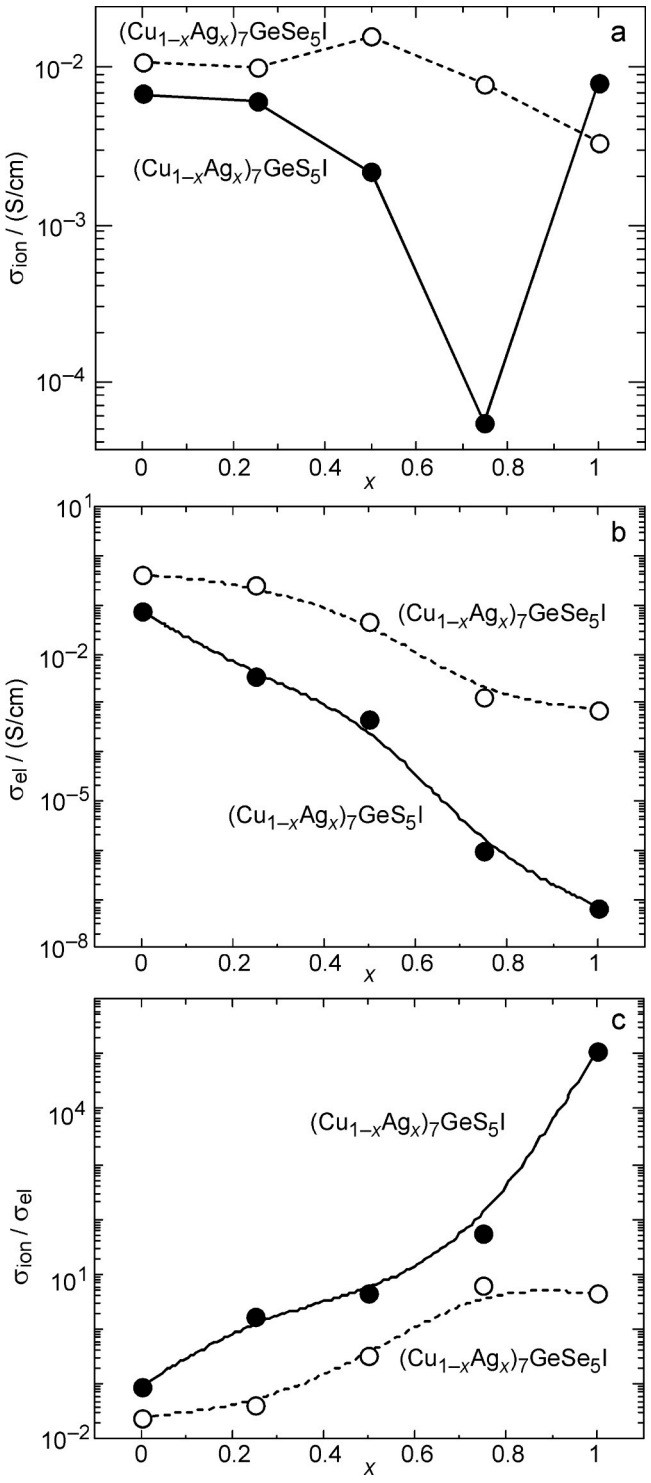

Fig. 6. Compositional dependences of ionic σ_{ion} (a) and electronic σ_{el} (b) conductivity as well as the ratio σ_{ion}/σ_{el} (c) at 298 K for $(Cu_{1-x}Ag_x)_7GeS_5I$ and $(Cu_{1-x}Ag_x)_7GeSe_5I$ mixed crystals. The experimental errors are below the symbol size.

(Se2Se2Se1I) with a displacement towards the Se2Se2Se1 and Se2Se1I1 triangle planes (Fig. 7a). In a solid solution silver is located both in Cu1 (24 g) and Cu2(48 h) positions with a displacement. The Cu1Ag1 position is located within the Se2Se2Se1 triangle plane, the Cu2Ag2 position is tetrahedrally coordinated (Se2Se2Se1I) with a strong displacement towards the ISe1 rib and the Se1ISe2 triangle plane for $(Cu_{0.75}Ag_{0.25})_7GeSe_5I$ or Se2I1Se2 plane for $(Cu_{0.5}Ag_{0.5})_7GeSe_5I$ (Fig. 7b). This leads to a strong disordering of the cation sublattice due to the introduction of Ag^+ ions and finally results in a splitting of the common Cu2Ag2 position, observed for $(Cu_{0.25}Ag_{0.75})_7GeSe_5I$. Ag_7GeSe_5I compound, similarly to Cu_7GeSe_5I, contains two symmetrically independent silver atoms in Ag1(24 g) and Ag2(48 h) positions, Ag1 being located in a trigonal coordination of se atoms Se2Se2Se1, while Ag2 atom is tetrahedrally coordinated (Se2Se2Se1I) with a slight displacement towards the planes of Se1Se2Se1 and Se2Se1I1 triangles (Fig. 7c).

Such features of the $Cu^+ \leftrightarrow Ag^+$ cationic substitution in the argyrodite structure for $(Cu_{1-x}Ag_x)_7GeSe_5I$ solid solutions affect the mechanism of the ionic conductivity. In Cu_7GeSe_5I and Ag_7GeSe_5I compounds mobile are Cu1 and Ag1 positions located in the trigonal coordination of selenium atoms. Mobile positions for the solid solutions are Ag1+Cu1 (trigonal coordination of selenium atoms for $(Cu_{0.75}Ag_{0.25})_7GeSe_5I$) and Ag2+Cu2 (tetrahedral coordination with displacement towards the [Se2I1Se2] triangle plane for $(Cu_{0.5}Ag_{0.5})_7GeSe_5I$ and $(Cu_{0.25}Ag_{0.75})_7GeSe_5I$) related to the cation sublattice disordering processes. In view of the above, we built compositional dependences of the mobile atom SOF (Fig. 4a) and the maximal distance between the CuAg mobile positions in the cationic sublattice (Fig. 4b).

It should be noted that the aforementioned compositional behaviour of the ionic and the electronic conductivity is in good agreement with the variation of both the $Cu^+(Ag^+)$ site mobilities and the distances between the corresponding mobile ion positions (Fig.4). For $(Cu_{1-x}Ag_x)_7GeSe_5I$ mixed crystals, the $Cu^+(Ag^+)$ cationic position mobilities decrease with respect to those of the end-point compounds. This corresponds to an increasing SOF for the mixed crystals in comparison with Cu_7GeSe_5I and Ag_7GeSe_5I [15]. Simultaneously, an increase of the distances between the mobile ion positions is observed, finally resulting in a corresponding minimum (Fig. 4b). For $(Cu_{1-x}Ag_x)_7GeSe_5I$ mixed crystals, on the contrary, an increasing mobility of the $Cu^+(Ag^+)$ cation sublattice positions (decreasing SOF) and decreasing distances between the mobile ion positions in the cationic sublattice are observed compared to the Cu_7GeSe_5I and Ag_7GeSe_5I crystals. This results in the maximum of the ionic conductivity for $(Cu_{0.5}Ag_{0.5})_7GeSe_5I$ [16]. Ag_7GeSe_5I and Ag_7GeSe_5I compounds are known to be characterised by the presence of symmetrically distinct Ag1 (24 g) and Ag2 (48 h) positions [15,16]. It is also worth notice that the value of the ionic conductivity component for Ag_7GeS_5I (7.98×10^{-3} S/cm) is higher than for Ag_7GeSe_5I (3.36×10^{-3} S/cm). This is also related to the structural features discussed above: the maximal distance d_{max} (Ag1–Ag1) for Ag_7GeS_5I is smaller than d_{max} (Ag1–Ag1) for Ag_7GeSe_5I (3.187 Å and 4.360 Å, respectively), the SOF (Ag1) value for Ag_7GeS_5I is smaller than SOF (Ag1) for Ag_7GeSe_5I (0.265 and 0.490, respectively).

The compositional behaviour of the electronic component of the conductivity (Fig.6b) for both $(Cu_{1-x}Ag_x)_7GeS_5I$ and $(Cu_{1-x}Ag_x)_7GeSe_5I$ systems is monotonous. Its values gradually decrease with $Cu^+ \rightarrow Ag^+$ substitution. Meanwhile, the electronic conductivity values for $(Cu_{1-x}Ag_x)_7GeS_5I$ mixed crystals are lower than for the selenium-containing counterparts. This is, first of all, related to differences in the band structure leading to a narrower bandgap for $(Cu_{1-x}Ag_x)_7GeSe_5I$ in comparison with $(Cu_{1-x}Ag_x)_7GeS_5I$. These differences are mainly related to the different properties of S^{2-} and Se^{2-} since the S→Se→Te row is characterised by increasing ionic radii ($r_i(S^{2-}) = 0.182$ nm, $r_i(Se^{2-}) = 0.193$ nm, $r_i(Te^{2-}) = 0.211$ nm). This reduces the ionisation energy, resulting, in turn, in an increasing amount of charge carriers in the conduction band.

It should be noted that the ionic-to-electronic component ratios for both $(Cu_{1-x}Ag_x)_7GeS_5I$ and $(Cu_{1-x}Ag_x)_7GeSe_5I$ mixed crystals exhibit monotonous increases (Fig.6c). Due to the lower electronic conductivity values for a number of $(Cu_{1-x}Ag_x)_7GeS_5I$ crystals, especially for Ag_7GeS_5I, the σ_{ion}/σ_{el} values are noticeably higher than for the similar selenium-containing compounds.

3.3. Raman scattering

Fig. 8 shows experimental Raman spectra of $(Cu_{1-x}Ag_x)_7GeS_5I$ and $(Cu_{1-x}Ag_x)_7GeSe_5I$ for different x values in panels (a) and (b), respectively. It is known that $Cu_{1-x}Ag_x)_7GeS_5I$ and $(Cu_{1-x}Ag_x)_7GeSe_5I$ mixed crystals are characterised by the $F\bar{4}3m$ space group belonging to the cubic crystal system [2]. The much more extensively studied Cu_6PS_5Hal (Hal = Cl, Br, I) argyrodites belong to the same symmetry group [2], hence it is reasonable to compare the Raman spectra of Fig. 6a with the Raman data for Cu_6PS_5Hal [21,22,24]. Note that all spectra in Fig. 6a were measured at a low laser power density P_{exc} (12 kW/cm^2). The Raman spectrum of Cu_7GeS_5I (bottom curve in Fig. 8a) is dominated by an intense relatively narrow (10 cm^{-1}) maximum near 407 cm^{-1}. It strongly resembles the case of Cu_6PS_5Hal with the most prominent peak observed near 425 cm^{-1} which corresponds to A_1-symmetry vibrations

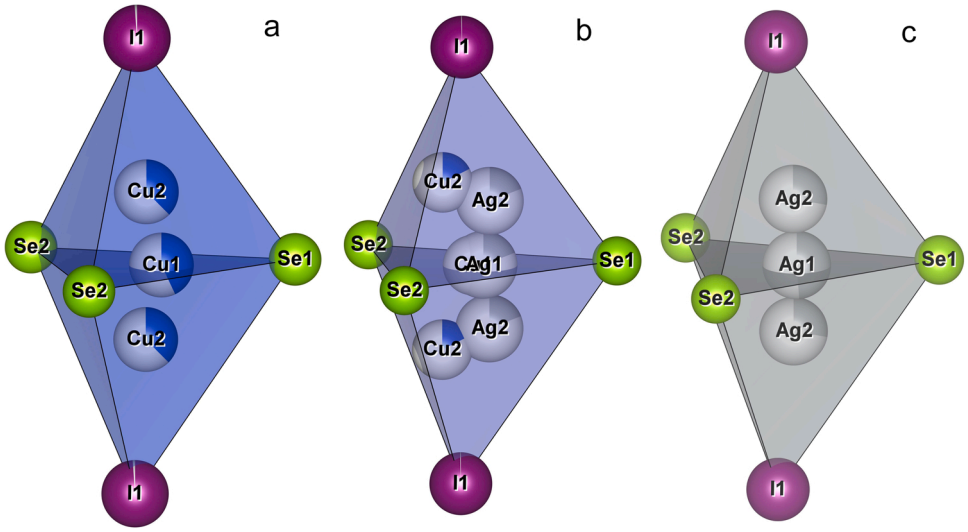

Fig. 7. Dynamics of $Cu^+ \leftrightarrow Ag^+$ subsitution in the Cu_7GeSe_5I–Ag_7GeSe_5I system through the example of $[Se_3I_2]$ doubled tetrahedra: (a) Cu_7GeSe_5I, (b) $(Cu_{0.5}Ag_{0.5})_7GeSe_5I$, and (c) Ag_7GeSe_5I.

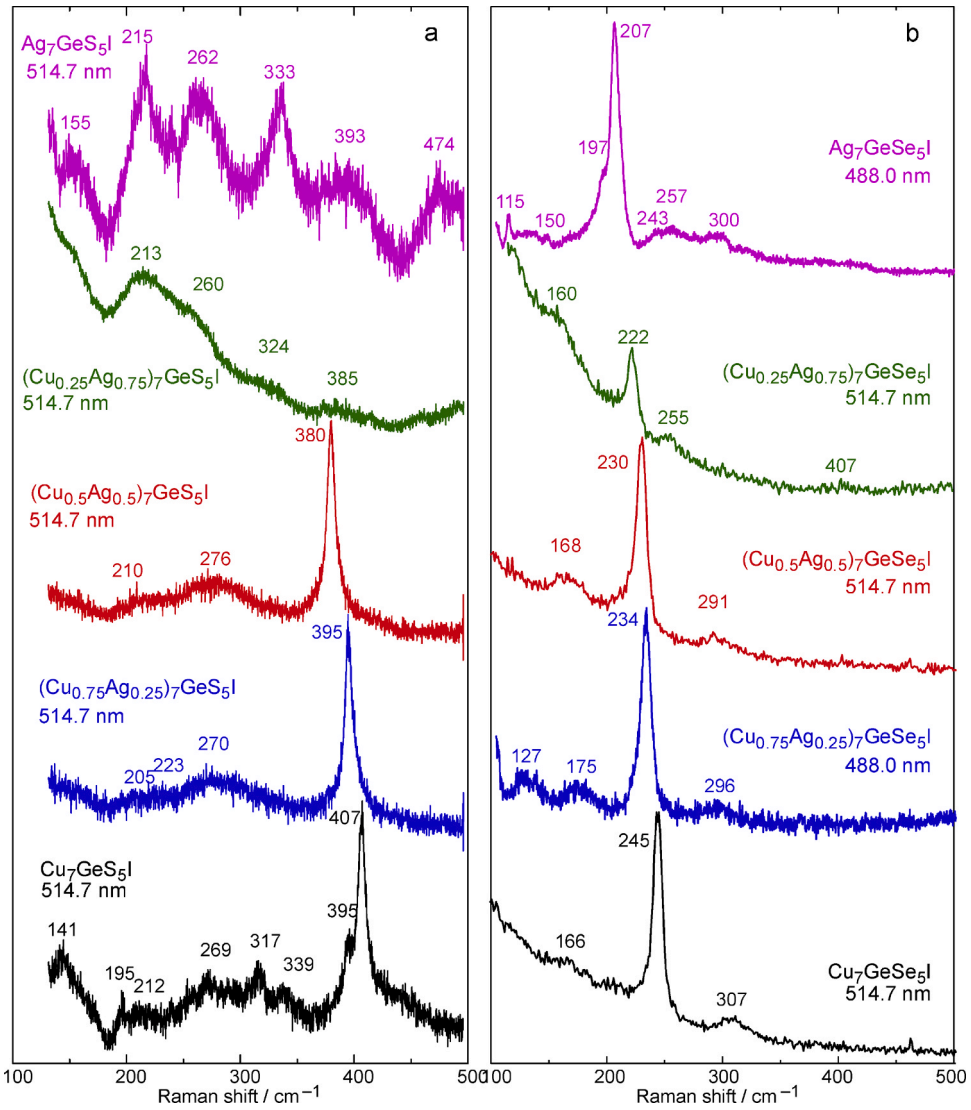

Fig. 8. Raman spectra of $(Cu_{1-x}Ag_x)_7GeS_5I$ (a) and $(Cu_{1-x}Ag_x)_7GeSe_5I$ (b) mixed crystals.

of PS_4 tetrahedra [21,22,24]. Consequently, we can ascribe the peak at 407 cm^{-1} in the Cu_7GeS_5I spectrum to similar vibrations of Ge–S bonds in GeS_4 tetrahedra. Even though a simple comparison of the square root of the GeS_4 and PS_4 tetrahedra mass ratio (1.12) and the inverse vibration frequency ratio (1.04) only shows a fair correlation, one should keep in mind that the relevant tetrahedra are not isolated in the argyrodite structure and evidently their vibration frequency does not depend solely on their mass. This is clearly confirmed by a quite significant downward shift of the discussed peak frequency with partial substitution of copper in Cu_7GeS_5I by heavier silver atoms: the corresponding intense narrow Raman peak is observed at 395 cm^{-1} for $(Cu_{0.75}Ag_{0.25})_7GeS_5I$ and at 380 cm^{-1} for $(Cu_{0.5}Ag_{0.5})_7GeS_5I$. This clearly indicates that Cu^+ or Ag^+ cations, external with respect to the GeS_4 tetrahedra, noticeably affect their dynamics. Note that no such effect was observed for phosphorus-based argyrodites when Cu^+ cations were replaced by lighter potassium species [36].

Lower-frequency Raman features in the $(Cu_{1-x}Ag_x)_7GeS_5I$ spectra are much less intense and broader. This is also typical for other argyrodites with cubic structure [21,22,24], hence their correct assignment is encumbered. As can be seen from Fig. 8a, partial Cu→Ag substitution results in an even stronger broadening of these features due to compositional disorder.

Further substitution of Cu by Ag unexpectedly leads to a dramatic change in the Raman spectra: for $(Cu_{0.25}Ag_{0.75})_7GeS_5I$ the Raman spectrum exhibits only a quite broad maximum at 213 cm^{-1} with weak shoulders at 260 cm^{-1} and 324 cm^{-1} while in the range of the expected prominent peak only a hardly visible broad feature near 385 cm^{-1} is revealed (Fig. 8a). It is reasonable to assume that such difference can be explained by some photochemical transformations in $(Cu_{0.25}Ag_{0.75})_7GeS_5I$ at P_{exc} value of 12 kW/cm^2 which does not lead to any noticeable damage of samples with lower silver content. A confirmation for the $(Cu_{1-x}Ag_x)_7GeS_5I$ surface degradation under laser illumination, especially at a higher power density, can be seen from Fig. 9 illustrating the rapid change of the Raman spectrum of a $(Cu_{0.5}Ag_{0.5})_7GeS_5I$ sample with increasing P_{exc}. Note that the initial spectrum shows only a partial recovery at a repeated measurement with reduced P_{exc} from the sample spot illuminated by a higher laser power density. Hence, the degradation of the sample surface under laser illumination is related to the $(Cu_{1-x}Ag_x)_7GeS_5I$ compound decomposition and formation of new phases. Note that examination of these new phases by X-ray diffraction is extremely problematic because the laser-induced transformations on the surface are strongly localised (the laser spot diameter is 1.3 μm).

It can be seen from Fig. 8a that for the $(Cu_{0.25}Ag_{0.75})_7GeS_5I$ crystal the laser-induced degradation of the Raman spectrum is observed already at minimal laser power density (12 kW/cm^2) and the spectrum evidently characterises not the $(Cu_{0.25}Ag_{0.75})_7GeS_5I$ crystal, but the

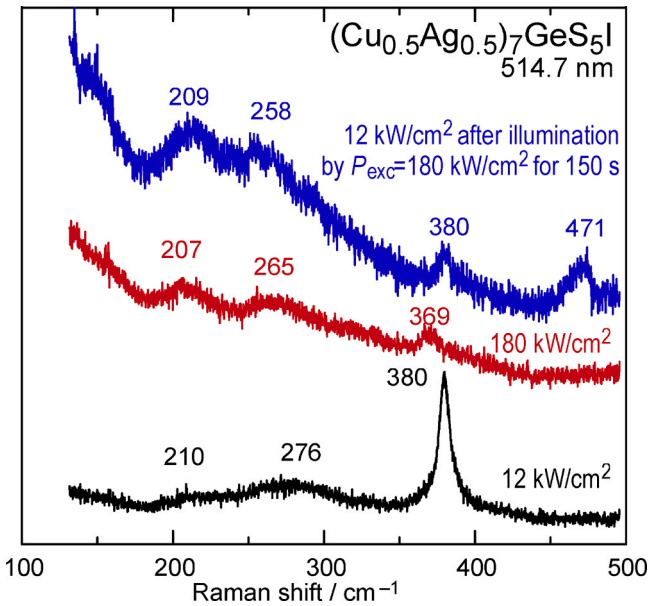

Fig. 9. Raman spectra of $(Cu_{0.5}Ag_{0.5})_7GeSe_5I$ mixed crystal at excitation with 514.7 nm laser line measured with different power densities $P_{exc.}$

products of a photochemical reaction on its surface. Generally, one can assume not only photochemical, but also thermochemical transformations or even evaporation of the sample material under laser beam. However, it was shown in our recent paper that at similar experimental conditions (the same LabRAM setup with the same 50x lens and the laser spot diameter of 1.3 μm at the laser wavelength 514.7 nm) the laser power density of 180 kW/cm^2 led to heating of a semiconductor chalcogenide sample with roughly similar absorption characteristics by nearly 100 K [37]. Hence, for 12 kW/cm^2 one should not expect the sample temperature at the laser spot to increase by more than 10 K, therefore thermochemical transformations at such experimental conditions are hardly possible. In particular, there is no chance for the material amorphisation or evaporation induced by the laser heating because the melting temperatures of the $(Cu_{1-x}Ag_x)_7GeS_5I$ crystals under study are above 1100 K.

The Ag_7GeS_5I spectrum, in particular the bandwidths and intensities of its features in Fig. 8a, can also be an evidence for photochemical changes on the crystal surface under laser irradiation. Note that the bands in the Ag_7GeS_5I spectrum are narrower than for $(Cu_{0.25}Ag_{0.75})_7GeS_5I$. In our opinion, this is related to the additional effect of compositional disorder in the $(Cu_{0.25}Ag_{0.75})_7GeS_5I$ mixed crystal.

The Raman spectra of $(Cu_{1-x}Ag_x)_7GeSe_5I$ mixed crystals (Fig. 8b) show that, at least at a first glance, these materials do not reveal noticeable degradation under laser irradiation during the Raman measurement. All spectra are typical for argyrodites, with the most intense narrow peak at 245 cm^{-1} for Cu_7GeSe_5I evidently corresponding to the vibrations of $GeSe_4$ tetrahedra. Similarly to the spectra of the $(Cu_{1-x}Ag_x)_7GeS_5I$ compounds (Fig. 8a), this peak shifts with Cu→Ag substitution gradually down to 207 cm^{-1} for Ag_7GeSe_5I. Such one-mode type compositional behaviour for the vibration of a pronounced structural group ($GeSe_4$ tetrahedron) is quite reasonable since the cation substitution occurs outside the $GeSe_4$ structural group and affects its vibrations as a whole contrary to the case of possible chalcogen substitution where one would expect a much more complicated compositional transformation similarly to the one observed for phosphorus-based complex chalcogenides and chalcohalogenides with pronounced PS_4 or PS_3 structural groups [21,38].

The compositional behaviour of the lower-frequency bands of $(Cu_{1-x}Ag_x)_7GeSe_5I$ as well as the weak higher-frequency maximum near 207 cm^{-1} can hardly be reliably traced because of their low intensity and large bandwidth.

Note, however, that the mentioned stability of $(Cu_{1-x}Ag_x)_7GeSe_5I$ compounds with respect to laser irradiation is somewhat questionable. Even though, as follows from Fig. 8b, the spectra of Ag-rich samples, contrary to their sulphur-based counterparts, do not exhibit distinctive features of surface degradation under laser irradiation, we observe that the Raman spectrum of Ag_7GeSe_5I strongly depends on the excitation wavelength λ_{exc} (Fig. 10). The most striking broader feature near 250 cm^{-1} in the spectrum under excitation with 514.7 nm, is most likely related to Se vibrations [39]. As in this case the most intense peak in the spectrum is revealed at 195 cm^{-1} that is quite away from the values of 207 cm^{-1} and 213 cm^{-1} where it is located at λ_{exc} = 488.0 nm and 632.8 nm, respectively, one must admit that the spectrum measured at 514.7 nm not merely contains a contribution from amorphous Se on the surface, but is most likely related to a different compound. Along with other differences in the Ag_7GeSe_5I spectra measured at different excitation wavelengths, this suggests that a more detailed study of the effect of λ_{exc} and P_{exc} on the Raman spectra of this compound is required.

4. Conclusions

Cu_7GeS_5I, Cu_7GeSe_5I, Ag_7GeS_5I, and Ag_7GeSe_5I crystals were grown by the directed crystallization while intermediate cation-substituted mixed crystals were grown by zone crystallization from the melt. The anionic core of the $(Cu_{1-x}Ag_x)_7GeS_5I$ and $(Cu_{1-x}Ag_x)_7GeSe_5I$ mixed crystals is built on the base of $[GeS_4]$ and $[GeSe_4]$, $[S_3I]$ and $[Se_3I]$, $[SI_4]$

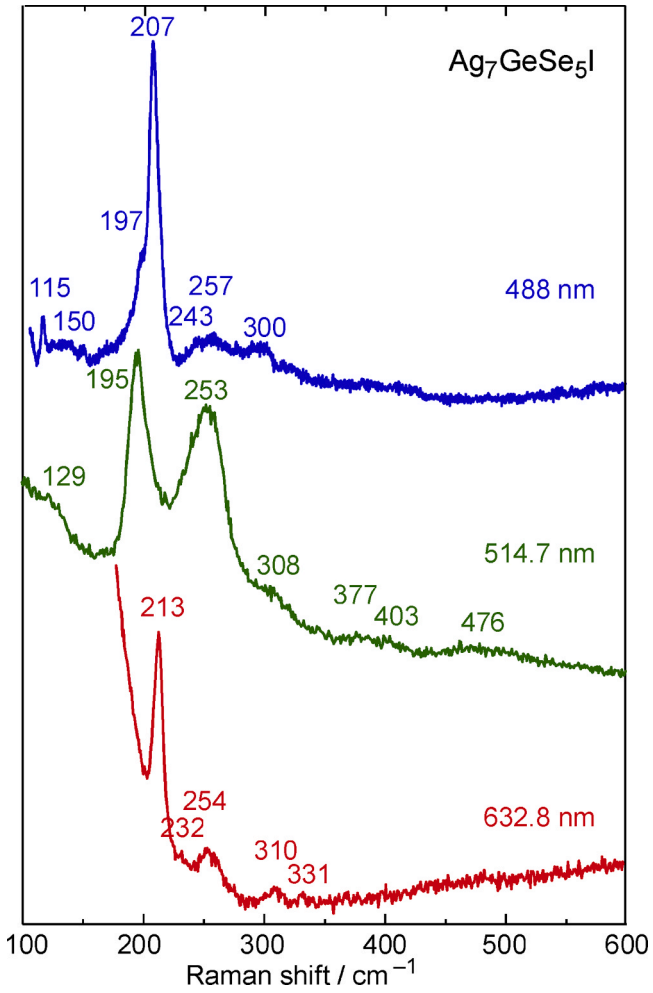

Fig. 10. Raman spectra of an Ag_7GeSe_5I crystal measured at different excitation wavelengths.

and [SeI_4] tetrahedra, on the faces and in the middle of which Cu and/or Ag atoms are located. The compositional dependence of the cubic lattice parameter for the $(Cu_{1-x}Ag_x)_7GeSe_5I$ mixed crystals is shown to be linear and to obey the Vegard law, while for the $(Cu_{1-x}Ag_x)_7GeS_5I$ crystals a slight downward bowing is observed. $Cu^+ \leftrightarrow Ag^+$ cationic substitution results in a monotonous variation of the anionic core while the cationic sublattice undergoes more complicated changes due to a nonlinear compositional behaviour of the SOF parameter an the distances between the $Cu^+(Ag^+)$ mobile ion positions in the $(Cu_{1-x}Ag_x)_7GeS_5I$ and $(Cu_{1-x}Ag_x)_7GeSe_5I$ mixed crystals.

Based on impedance measurements, the compositional dependences of the ionic and electronic components of the electrical conductivity for $(Cu_{1-x}Ag_x)_7GeS_5I$ and $(Cu_{1-x}Ag_x)_7GeSe_5I$ are obtained. A non-monotonous compositional behaviour of the ionic conductivity is observed with a minimum at $x = 0.75$ for $(Cu_{1-x}Ag_x)_7GeS_5I$ and a maximum at $x = 0.5$ for $(Cu_{1-x}Ag_x)_7GeSe_5I$. Such behaviour is in good agreement with the compositional variation of the mobility of the $Cu^+(Ag^+)$ positions and variation of the distances between the corresponding mobile ion positions in the cationic sublattice. The electronic component of the conductivity is higher for the $(Cu_{1-x}Ag_x)_7GeSe_5I$ crystals than for their sulphur-based counterparts and gradually decreases with $Cu^+ \rightarrow Ag^+$ substitution. Besides, the cationic $Cu^+ \rightarrow Ag^+$ substitution results in an increase of the ionic-to-electronic conductivity ratio, the latter being higher for $(Cu_{1-x}Ag_x)_7GeS_5I$ than for the selenium-containing crystals.

The first Raman spectroscopic study of $(Cu_{1-x}Ag_x)_7GeSe_5I$ and $(Cu_{1-x}Ag_x)_7GeSe_5I$ mixed crystals is consistent with the XRD data on their cubic structure, similar to phosphorus-based copper-containing superionic argyrodites. The compositional behaviour of the most prominent peak (corresponding to the vibrations of GeS_4 or $GeSe_4$ tetrahedra) under Cu→Ag cation substitution is one-mode, which is quite reasonable since the substitution occurs outside the pronounced structural group. However, the unexpectedly strong shift of the peak frequency with x leads to the conclusion that the replacement of copper by heavier silver cations noticeably affects the dynamics of GeS_4 or $GeSe_4$ tetrahedra. Compounds with high silver content (especially in the germanopentasulphoiodide system) easily undergo photochemical surface transformations under laser irradiation during the Raman measurements which require a detailed targeted study.

CRediT authorship contribution statement

I.P. Studenyak: Supervision. **A.I. Pogodin:** Investigation, Visualization, Writing - original draft. **V.I. Studenyak:** Software, Validation. **M.J. Filep:** Data curation, Visualization, Writing - original draft. **O.P. Kokhan:** Conceptualization, Methodology. **P. Kúš:** Conceptualization, Methodology. **Y.M. Azhniuk:** Visualization, Investigation, Writing - original draft. **D.R.T. Zahn:** Writing - review & editing.

Declaration of Competing Interest

The authors of manuscript entitled “Structure, electrical conductivity, and Raman spectra of $(Cu_{1-x}Ag_x)_7GeS_5I$ and $(Cu_{1-x}Ag_x)_7GeSe_5I$ mixed crystals” declare no conflicts of interest.

Acknowledgement

Y.M. Azhniuk is grateful to Chemnitz University of Technology (Visiting Scholar Program) for the financial support of his research stay at the university.

References

[1] W.F. Kuhs, R. Nitsche, K. Scheunemann, The argyrodites – a new family of the tetrahedrally close-packed structures, Mat. Res. Bull. 14 (1979) 241–248.
[2] T. Nilges, A. Pfitzner, A structural differentiation of quaternary copper argyrodites: structure – property relations of high temperature ion conductors, Z. Kristallogr. 220 (2005) 281–294.
[3] S. Boulineau, M. Courty, J.-M. Tarascon, V. Viallet, Mechanochemical synthesis of Li-argyrodite Li_6PS_5X (X=Cl, Br, I) as sulfur-based solid electrolytes for all solid state batteries application, Solid State Ion. 221 (2012) 1–5.
[4] S. Yubuchi, S. Teragawa, K. Aso, K. Tadanaga, A. Hayashi, M. Tatsumisago, Preparation of high lithium-ion conducting Li_6PS_5Cl solid electrolyte from ethanol solution for all-solid-state lithium batteries, J. Power Sources 293 (2015) 941–945.
[5] C. Yu, L. van Eijck, S. Ganapathy, M. Wagemaker, Synthesis, structure and electrochemical performance of the argyrodite Li_6PS_5Cl solid electrolyte for Li-ion solid state batteries, Electrochim. Acta 215 (2016) 93–99.
[6] N.C. Rosero-Navarro, T. Kinoshita, A. Miura, M. Higuchi, K. Tadanaga, Effect of the binder content on the electrochemical performance of composite cathode using Li_6PS_5Cl precursor solution in an all-solid-state lithium battery, Ionics 23 (2017) 1619–1624.
[7] S. Wenzel, S.J. Seldmaier, C. Dietrich, W.G. Zeier, J. Janek, Interfacial reactivity and interphase growth of argyrodite solid electrolytes at lithium metal electrodes, Solid State Ion. 318 (2018) 102–112.
[8] Z. Zhang, L. Zhang, X. Yan, H. Wang, Y. Liu, C. Yu, X. Cao, L. van Eijck, B. Wen, All-in-one improvement toward Li_6PS_5Br-based solid electrolytes triggered by compositional tune, J. Power Sources 410–411 (2019) 162–170.
[9] I.P. Studenyak, M. Kranjčec, Gy.Sh. Kovacs, I.D. Desnica-Frankovic, A.A. Molnar, V.V. Panko, V.Yu. Slivka, Electrical and optical absoprtion studies of Cu_7GeS_5I fast-ion conductor, J. Phys.Chem. Solids 63 (2002) 267–271.
[10] A.F. Orliukas, E. Kazakevicius, A. Kezionis, T. Salkus, I.P. Studenyak, R. Yu. Buchuk, I.P. Prits, V.V. Panko, Preparation, electric conductivity and dielectrical properties of Cu_6PS_5I-based superionic composites, Solid State Ion. 180 (2009) 183–186.
[11] I.P. Studenyak, M. Kranjčec, V.V. Bilanchuk, O.P. Kokhan, A.F. Orliukas, E. Kazakevicius, A. Kezionis, T. Salkus, Temperature variation of electrical conductivity and absorption edge in Cu_7GeSe_5I advanced superionic conductor, J. Phys.Chem. Solids 70 (2009) 1478–1481.
[12] T. Šalkus, E. Kazakevičius, J. Banys, M. Kranjčec, A.A. Chomolyak, Yu.Yu. Neimet, I.P. Studenyak, Influence of grain size effect on electrical properties of Cu_6PS_5I superionic ceramics, Solid State Ion. 262 (2014) 597–600.
[13] R. Belin, L. Aldon, A. Zerouale, C. Belin, M. Ribes, Crystal structure of the non-stoichiometric argyrodite compound $Ag_{7-x}GeSe_5I_{1-x}$ ($x = 0.31$). A highly disordered silver superionic conducting material, Solid State Sci. 3 (2001) 251–265.
[14] S. Albert, S. Pillet, C. Lecomte, A. Pradel, M. Ribes, Disorder in Ag_7GeSe_5I, a superionic conductor: temperature-dependent anharmonic structural study, Acta Crystallographica B 64 (2008) 1–11.
[15] I.P. Studenyak, A.I. Pogodin, O.P. Kokhan, V. Kavaliukė, T. Šalkus, A. Kežionis, A. F. Orliukas, Crystal growth, structural and electrical properties of $(Cu_{1-x}Ag_x)_7GeS_5I$ superionic solid solutions, Solid State Ion. 329 (2019) 119–123.
[16] I.P. Studenyak, A.I. Pogodin, M.M. Luchynets, V.I. Studenyak, O.P. Kokhan, P. Kúš, Impedance studies and electrical conductivity of $(Cu_{1-x}Ag_x)_7GeSe_5I$ mixed crystals, J. Alloys. Compd. 817 (2020), 152792.
[17] I.P. Studenyak, V.Yu. Izai, V.I. Studenyak, O.V. Kovalchuk, T.M. Kovalchuk, P. Kopčanský, M. Timko, N. Tomašovičová, V. Zavisova, J. Miskuf, I.V. Oleinikova, Influence of Cu_6PS_5I superionic nanoparticles on the dielectric properties of 6CB liquid crystal, Liq. Cryst. 44 (2017) 897–903.
[18] I.P. Studenyak, M. Kranjčec, V.Yu. Izai, A.A. Chomolyak, M. Vorohta, V. Matolin, C. Cserhati, S. Kökényesi, Structural and temperature-related disordering studies of Cu_6PS_5I amorphous thin films, Thin Solid Films 520 (2012) 1729–1733.
[19] I.P. Studenyak, O.P. Kokhan, M. Kranjčec, V.V. Bilanchuk, V.V. Panko, Influence of S→Se substitution on chemical and physical properties of $Cu_7Ge(S_{1-x}Se_x)_5I$ superionic solid solutions, J. Phys.Chem. Solids 68 (2007) 1881–1884.
[20] I.P. Studenyak, M. Kranjčec, V.V. Bilanchuk, O.P. Kokhan, A.F. Orliukas, A. Kezionis, E. Kazakevicius, T. Salkus, Temperature and compositional behaviour of electrical conductivity and optical absorption edge in $Cu_7Ge(S_{1-x}Se_x)_5I$ mixed superionic crystals, Solid State Ion. 181 (2010) 1596–1600.
[21] I.P. Studenyak, V.O. Stefanovich, M. Kranjčec, I.D. Desnica, Yu.M. Azhnyuk, Gy. Sh. Kovacs, V.V. Panko, Raman scattering studies of Cu_6PS_5Hal (Hal=Cl,Br,I) fast-ion conductors, Solid State Ion. 95 (1997) 221–225.
[22] M. Kranjčec, I.P. Studenyak, R.Yu. Buchuk, V.O. Stephanovich, S. Kökényesi, M. Kis-Varga, Structural properties and Raman scattering in Cu_6PS_5X (X=I, Br) nanocrystalline solid electrolytes, Solid State Ion. 179 (2008) 218–221.
[23] B. Graeser, R. Agrawal, Pure phase synthesis of Cu_3PS_4 and Cu_6PS_5Cl for semiconductor applications, RSC Adv. 8 (2018) 34094–34101.
[24] I.P. Studenyak, M.M. Luchynets, V.Yu Izai, A.I. Pogodin, O.P. Kokhan, Yu. M. Azhniuk, D.R.T. Zahn, Structural properties, Raman spectra, and diffuse reflectivity of $(Cu_6PS_5Br)_{1-x}(Cu_7PS_6)_x$ mixed crystals, J. Alloys. Compd. 782 (2019) 586–591.
[25] H.M. Rietveld, A profile refinement method for nuclear and magnetic structures, J. Appl. Crystallogr. 2 (1969) 65–71.
[26] L.B. McCusker, R.B. Von Dreele, D.E. Cox, D. Louër, P. Scardi, Rietveld refinement guidelines, J. Appl. Crystallogr. 32 (1999) 36–50.
[27] A. Altomare, M.C. Burla, M. Camalli, B. Carrozzini, G. Cascarano, C. Giacovazzo, A. Guagliardi, A.G.G. Moliterni, G. Polidori, R. Rizzi, EXPO: a program for full powder pattern decomposition and crystal structure solution, J. Appl. Crystallogr. 32 (1999) 339–340.
[28] A. Altomare, C. Cuocci, C. Giacovazzo, A. Moliterni, R. Rizzi, N. Corriero, A. Falcicchio, EXPO2013: a kit of tools for phasing crystal structures from powder data, J. Appl. Crystallogr. 46 (2013) 1231–1235.

[29] K. Momma, F. Izumi, VESTA 3 for three-dimensional visualization of crystal, volumetric and morphology data, J. Appl. Crystallogr. 44 (2011) 1272–1276.
[30] A. Nagel, K.-J. Range, Verbindungsbildung im system Ag_2S–GeS_2–AgI, Z. Naturforsch. 33b (1978) 1461–1464.
[31] A. Nagel, K.-J. Range, Die Kristallstruktur von Ag_7GeS_5I, Z. Naturforsch. (1979) 360–362. – 34b. – P.
[32] L. Aldon, R. Belin, Y. Pontillon, Neutron crystal structure of heptasilver(I) tetraseleniogermanate(IV) selenide iodide, Ag_7GeSe_5I, Z. Kristallogr, – New Crystal Structures 216 (2001) 181–182.
[33] I.P. Studenyak, V.Yu. Izai, V.I. Studenyak, A.I. Pogodin, M.Y. Filep, O.P. Kokhan, B. Grančič, P. Kúš, Interrelations between structural and optical properties of $(Cu_{1-x}Ag_x)_7GeS_5I$ mixed crystals, Ukr. J. Phys. Opt. 19 (2018) 237–243.
[34] R.A. Huggins, Simple method to determine electronic and ionic components of the conductivity in mixed conductors: a review, Ionics 8 (2002) 300–313.
[35] A.R. West, Solid State Chemistry and Its Applications, second ed., John Wiley & Sons, 2014.
[36] I.P. Studenyak, A.I. Pogodin, V.I. Studenyak, O.P. Kokhan, Yu.M. Azhniuk, C. Cserháti, S. Kökényesi, D.R.T. Zahn, Synthesis and characterisation of new potassium-containing argyrodite-type compounds, Semicond. Phys., Quantum Electron. & Optoelectron. 22 (2019) 26–33.
[37] Yu.M. Azhniuk, D. Solonenko, V.Yu. Loya, V.M. Kryshenik, V.V. Lopushansky, A. Mukherjee, A.V. Gomonnai, D.R.T. Zahn, Flexoelectric and local heating effects on CdSe nanocrystals in amorphous As_2Se_3 films, Mater. Res. Expr. 6 (2019), 095913.
[38] A.V. Gomonnai, Yu.M. Vysochanskii, M.I. Gurzan, V.Yu. Slivka, Lattice-dynamics of ferroelectric $Sn_2P_2(Se_xS_{1-x})_6$ solid solutions, Sov. Phys. Solid State 25 (1983) 835–839.
[39] S. Yannopoulos, Structure and photo-induced effects in elemental chalcogens: a review on Raman scattering, J. Mater. Sci.: Materials in Electronics (2020), https://doi.org/10.1007/s10854-020-03310-0.